Sixth International Symposium on Turbulence and Shear Flow Phenomena
Seoul, Korea, 22-24 June 2009

EFFECT OF ROTOR BLADE SCALING ON GAS TURBINE PERFORMANCE

Derek Lastiwka
Dongil Chang
Stavros Tavoularis
Department of Mechanical Engineering,
University of Ottawa
Ottawa, ON K1N 6N5, Canada
stavros.tavoularis@uottawa.ca

ABSTRACT

The present work is a study of the effects of rotor blade scaling of a single-stage high pressure turbine on the time-averaged turbine performance and on parameters that influence vibratory stresses on the rotor blades. Three configurations have been considered: a reference case with 36 rotor blades and 24 stator vanes, a case with blades upscaled by 12.5%, and a case with blades downscaled by 10%. The present results demonstrate that blade scaling effects were essentially negligible on the time-averaged turbine performance, but measurable on the unsteady surface pressure fluctuations, maximum levels of which occurred near the leading edges and towards the roots of the blades.

INTRODUCTION

A common approach in computational fluid dynamics (CFD) is to take advantage of existing geometric periodicity in order to reduce the required computer memory, storage space and computational time. In such cases, only one of the repeated sections of the domain is considered and periodic boundary conditions are applied at its boundaries.

In the case of turbine stages, which consist of successive rows of stator vanes and rotor blades, azimuthal periodicity would occur when the ratio of the number of rotor blades and stator vanes is equal to the ratio of two small integers. In practice, however, this is rarely the case, which implies that accurate simulation of turbine stages would require consideration of the entire stator and rotor. To circumvent this problem, turbine analysts have used several different methods including rotor blade scaling (Rai, 1987; Rai and Madavan, 1990), phase lagged periodic boundary conditions, and time inclined boundary conditions. Unlike the two other methods, the rotor blade scaling technique requires no modifications to existing CFD codes and has been widely used in numerous published papers. Therefore, the rotor blade scaling method was chosen for this study.

Yao et al. (2002) noted that, when comparing simulations for an unscaled turbine and for one with blades scaled down by 14%, the time-averaged pressure and the peak-to-peak pressure variations were nearly the same, which led to approximate equality of the torques produced by the two turbines. If the rotational speed were also kept unchanged during scaling, then the power output of the scaled turbine would be equal to that of the unscaled one. Clark et al. (2000) studied the blade scaling effects on the pressure fluctuation spectrum by upsizing the rotor blade by 3.7%. They found that, by comparison to the unscaled case, the peak amplitude at the fundamental blade passing frequency for the upscaled blade was higher, whereas the peak amplitudes at higher frequency harmonics were lower. The findings of these two previous studies are not conclusive, because each considered only one scaled case for their comparisons. A more complete study should consider scaling effects with both downsizing and upsizing the blades.

The objective of the present study is to determine the quantitative effects that rotor blade scaling has on the numerical simulations of a representative single-stage gas turbine, with particular focus on parameters that influence vibratory stresses on the rotor blades.

ROTOR BLADE SCALING

The rotor blade scaling simplifies the computational geometry by changing the number of blades such that the blade-to-vane ratio Λ_s in the scaled geometry is equal to the ratio of two small integers (e.g., 1/1, 1/2, 1/3, 2/3, 3/4 etc.).

An approach referred to as *rotor blade scaling* (Rai, 1987; Rai and Madavan, 1990) has been adopted to permit simulations using relatively small periodic domains. During scaling, it is desirable to maintain the airfoil shape intact as well as to preserve the power generated by the original rotor (Yao et al., 2002). This requires that the rotor blade pitch-to-chord ratio (solidity ratio) be kept constant, which is achieved by scaling the rotor blade by the scaling ratio factor, defined as

$$q = \frac{\Lambda}{\Lambda_s} \tag{1}$$

where the ratio of the number of rotor blades N_r and the number of stator vanes N_s is $\Lambda = N_r / N_s$.

The chord length C_s of the scaled rotor blade is then adjusted as

$$C_s = q\ C \tag{2}$$

where C is the chord length of the unscaled rotor blade. Similarly, the scaled rotor blade pitch $L_{rp,s}$ is adjusted as

$$L_{rp,s} = q\, L_{rp} \tag{3}$$

where L_{rp} is the unscaled rotor blade pitch.

The unscaled turbine geometry used in the present study was provided by the Institute for Thermal Turbomachinery and Machine Dynamics (TTM), Graz University of Technology, Austria (Göttlich et al., 2004). Two scaled turbine geometries were obtained by multiplying the tangential and axial coordinates of the blades by the scaling ratio, while leaving the radial coordinates unchanged. Thus, the blade height, like the casing and hub locations were the same for all cases. Table 1 summarizes the scaling values for the three turbine configurations, whereas Fig. 1 compares the profiles of the three blades at midspan. During scaling, the axial gap distance between the rotor and the stator were kept constant by shifting the scaled geometries in the axial and tangential directions such that the leading edges of the scaled blades (TTM4:3 and TTM5:3) were aligned with the leading edges of the unscaled blades (TTM3:2), as shown in Fig.1.

A consequence of blade scaling as described previously would be a change in the rotor tip gap height, which would not be acceptable as it would affect the tip losses and turbine efficiency. To avoid this problem, the radial coordinates of the blade defining the tip were adjusted such as to maintain the tip gap unchanged by scaling.

Table 1: Scaling parameters of the three turbine configurations

Case	N_{rt}	N_{st}	Λ	q	scaling
TTM4:3	32	24	1.333	1.125	+12.5%
TTM3:2	36	24	1.500	1.000	unscaled
TTM5:3	40	24	1.667	0.900	-10.0%

In the present work, solely because of the availability of experimental results, the *unscaled* TTM3:2 geometry was used as the reference, although it requires a smaller computational domain than the "scaled" cases TTM5:3 and TTM4:3. In practice, the situation would likely be reversed. One would have a reference case (TTM5:3 or TTM4:3) with a larger computational domain. In turn, one would perform rotor blade scaling to get a scaled case (TTM3:2). If so, the scaling ratio would be changed to 0.889 for TTM4:3 and 1.111 for TTM5:3.

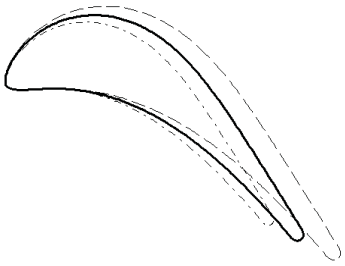

Fig. 1: Blade profiles at mid span: - - - - TTM4:3, ——— TTM3:2, — - — TTM5:3.

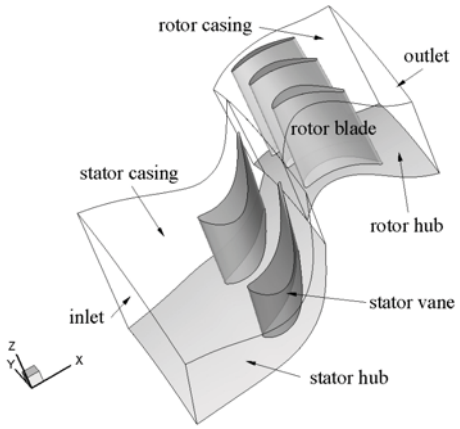

Fig. 2: Computational domain of the TTM turbine stage for the unscaled case (TTM3:2).

COMPUTATIONAL PROCEDURES

Simulations were conducted using the commercial software FLUENT 6.3.26. The density-based solver was used due to the compressible nature of the flow in the turbine. The Unsteady Reynolds-averaged Navier-Stokes (URANS) equations were solved with the SST (Shear Stress Transport) turbulence model (Menter, 1991).

For high accuracy, a second-order upwind scheme and a second-order implicit Euler scheme were used for spatial and temporal discretizations, respectively. After reviewing the various available schemes, it was concluded that these second order schemes are good compromises between accuracy and numerical stability. In all simulations, the specific heat, the thermal conductivity, and the viscosity were assumed to be constant across the turbine stage.

Figure 2 shows the computational domain of the unscaled case (TTM3:2), which is divided into two subdomains, with the rotor domain rotating while the stator domain remains stationary. Rotationally periodic boundary conditions (side planes of each domain) were used to reduce the size of the computational domain to a 1/12th sector. The total pressure and the total temperature were specified at the inlet, while the static pressure was set on the hub line of the outlet plane. The static pressure distribution at the outlet was obtained by using the radial equilibrium relation. Unsteady simulations using 800 time steps per blade passage past each vane were found to adequately resolve unsteady effects of interest in this work.

The degree of convergence of the present simulations to a periodic state was determined following the procedure of Clark and Grover (2007). As our focus is on parameters that influence vibratory stresses on the rotor blades, the temporal fluctuations of the static pressure on the blade surface were used for the estimation of the convergence level of the simulations. The pressure on the suction side of the blade at 10% span and 10% axial chord was selected as the approximate location of strongest pressure fluctuations (see next section). The overall convergence level was calculated as the minimum value among the convergence levels of the pressure averaged over one vane passing period τ_v (namely, the time it takes for one blade to advance from one vane location to the next), the cross-correlation factor (CCF) at zero lag, and the fractional power of the power spectrum. The overall convergence level reached the value 0.988 for the unscaled case (TTM3:2), which is higher than the threshold of 0.950 suggested by Clark and Grover (2007) to be sufficient. All data used during post-processing were collected during the final cycle of the simulations.

RESULTS AND DISCUSSION

Table 2 compares the values of some important time-averaged turbine performance parameters for the three cases considered. These include the normalized turbine power, the total-to-total turbine efficiency, the total pressure ratio, and the total temperature drop across the turbine stage. The normalized turbine power is defined as

$$W = \frac{\dot{m}\, c_p \left(T_{03} - T_{02}\right)}{P_{01}\, D_{hub}^2 \sqrt{\mathrm{R} T_{01}}} \tag{4}$$

where $\dot{m}$ is the mass flow rate through the turbine stage; c_p is the specific heat capacity under constant pressure; T_{03}, T_{02} and T_{01} are the total temperatures at the rotor outlet, the stator outlet, and the inlet, respectively; P_{01} is the total pressure at the inlet; R is the gas constant of air; and D_{hub} is the rotor hub diameter. The total-to-total turbine efficiency is defined as (γ is the specific heat ratio)

$$\eta_{tt} = \frac{T_{01} - T_{03}}{T_{01}\left[1 - \left(\frac{P_{03}}{P_{01}}\right)^{(\gamma-1)/\gamma}\right]} \tag{5}$$

Table 2: Normalized time averaged turbine performance parameters

	W	η_{tt}	$\frac{P_{01}}{P_{03}}$	$\frac{\left(T_{01} - T_{03}\right)}{T_{03}}$
TTM4:3	0.0984 (+0.24%)	0.878 (-0.38%)	3.198 (+0.22%)	0.2481 (+0.22%)
TTM3:2	0.0982	0.884	3.180	0.2487
TTM5:3	0.0980 (-0.19%)	0.881 (-0.02%)	3.175 (-0.50%)	0.2477 (-0.39%)

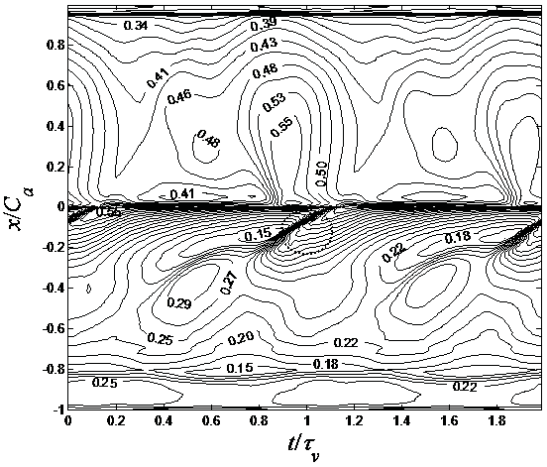

Fig. 3: Non-dimensionalized surface pressure P/P_{01} on the unscaled blade at 10% span; positive x/c_a indicates the pressure side, whereas negative x/c_a indicates the suction side; an ellipse marks a possible shock location.

These results clearly demonstrate that the rotor blade scaling had a negligible effect on the time-averaged turbine performance. This is consistent with our expectations, because the rotor solidity, the ratio of the tip clearance height and the blade height, and the axial gap size were the same for all examined cases.

The surface pressure on the unscaled blade at 10% span of a rotor blade is plotted against time in Fig. 3; in this figure, time has been normalized by the vane passing period τ_v, pressure has been normalized by the total inlet pressure P_{01}, and axial distance has been normalized by the axial chord C_a. Strong shocks originating on the trailing edge of the upstream stator vane are seen to first touch on the suction side of the blade at 20% axial chord and, as time passes, to move toward the leading edge. This figure also clearly illustrates the strong periodicity of the time-varying pressure over two consecutive vane passing periods.

Figure 4 shows the variation of the dimensionless time-averaged surface static pressure at three different spanwise locations of the blade. It can be seen that the time-averaged blade loading increases from the rotor hub towards the blade tip. The same figure also indicates that the impingement of vane trailing edge shocks on the suction side of the blades is mostly confined in the lower (10% span) and the front part (between the leading edge and the 20% axial chord position) of the blade. According to McBean et al. (2005), the passage shocks can be identified by the local minimum pressure. Passage shocks are located at 80% axial chord for the 10% and 50% spans. Differences in pressure distributions among the three cases studied are relatively small. Compared to the unscaled case (TTM3:2), the local pressure is lower in the upscaled case (TTM4:3) and higher in the downscaled case (TTM5:3) for the most part of the blade span, except in the aft-section of the blade suction side (from 80% of the axial chord to the trailing edge of the blade).

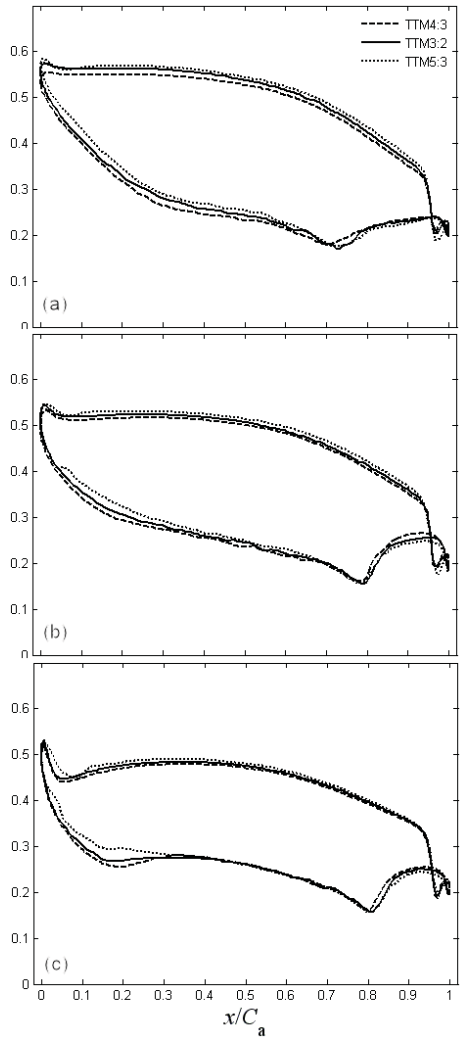

Fig. 4: Dimensionless time-averaged static pressure $\overline{P}/P_{01}$ on the blade at 90% (a), 50% (b), 10% (c) spans.

Figure 5 shows iso-contours of the standard deviation of the pressure fluctuations on the suction side of the blade, where they are strongest. The strongest fluctuations occur near the leading edge (at approximately 10% axial chord) and toward the rotor hub (at approximately 10% span), where the influence of the vane trailing edge shocks is also strongest (see Fig. 3). It is seen in Fig. 5 that the maximum standard deviation of pressure fluctuations in the front part of the blade increases as the number of blades is reduced during scaling.

Figure 6 shows the variation of the local standard deviation of static pressure fluctations on the suction side of the blade at 10% span. As also seen in Fig. 5, the strongest pressure fluctuations occur near the 10% axial chord location in all cases. In general, in the front part of the blade, pressure fluctuations in the upscaled case (TTM4:3) are somewhat stronger than those in the unscaled case (TTM3:2) whereas in the downscaled case (TTM5:3) they are somewhat weaker than in the unscaled case.

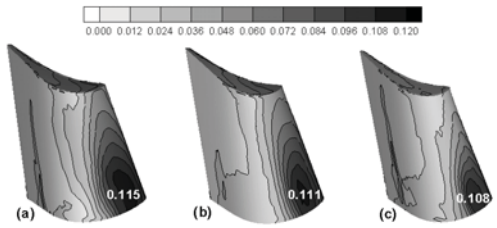

Fig. 5: Iso-contours of the standard deviation of static pressure fluctuations (normalized by total inlet pressure) on the suction side of the blade: (a) TTM4:3, (b) TTM3:2, (c) TTM5:3.

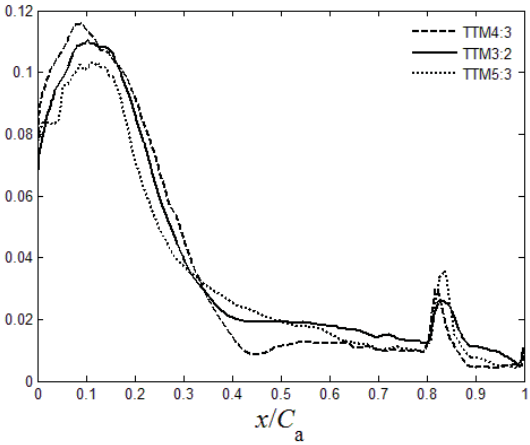

Fig. 6: Standard deviation of static pressure fluctuations normalized by the total inlet pressure on the suction side of the blades at 10% span.

The influence of scaling on the pressure fluctuations in the middle and the aft sections of the blade is not easy to explain, however, this is not of much concern as the levels of these fluctuations are all relatively low.

Figure 7 shows the spectral amplitude of the static pressure fluctuations at 10% span and 10% axial chord. Both downsizing the rotor blade by 10% (TTM5:3) and upsizing the rotor blade by 12.5% (TTM4:3) left unchanged the fundamental vane passing frequency f_v and its harmonics. This is consistent with expectations, because the rotor blades pass the stator vanes at the same rotational speed. Nevertheless, downsizing the blades (TTM4:3) increased the peak amplitude of the pressure fluctuations on the rotor blade at the fundamental vane frequency, while upsizing the blades (TTM5:3) decreased the peak amplitude of the pressure fluctuations. Figure 7 clearly shows that the spectral peaks decrease from the fundamental frequency towards the higher harmonics, but also that harmonics up to at least order 10 have a non-negligible proportion of the total power. In this figure, the effect of scaling is visible on the fundamental frequency peak but hard to discern for the other harmonics.

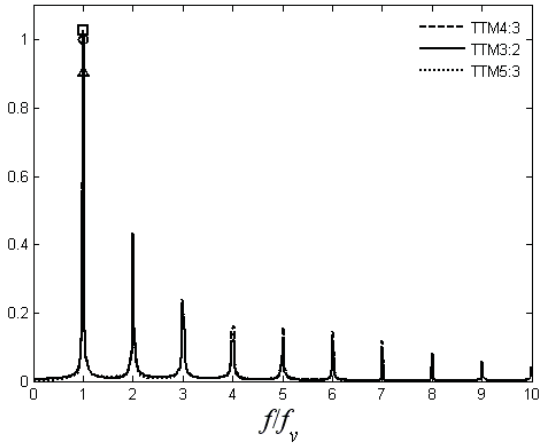

Fig. 7: Spectral amplitude (normalized by its value in the TTM3:2 case at the fundamental stator vane passing frequency) of pressure fluctuations on the suction side of a rotor blade at 10% span and 10% axial chord; □ TTM4:3, ○ TTM3:2, Δ TTM5:3.

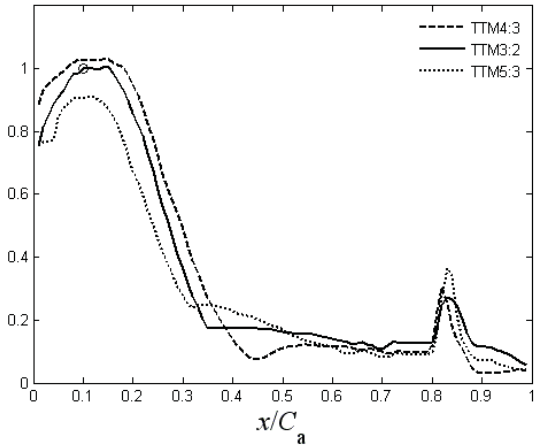

Fig. 8: Spectral amplitude (normalized by its value in the TTM3:2 case at the fundamental stator vane passing frequency) of pressure fluctuations at the fundamental stator vane passing frequency on the suction side of a rotor blade at 10% span.

Figure 8 shows that the variation of the spectral peak amplitude at the fundamental frequency along the suction side of the blade at 10% span is similar to that of the standard deviation of the pressure fluctuations, shown in Fig. 6, as expected by considering that much of the spectral power is at the fundamental frequency.

Figure 9 shows the influence of the scaling ratio factor on the peak amplitudes of pressure fluctuations at the fundamental vane frequency for three different spanwise locations. By reference to the unscaled case, the changes in the amplitudes of the spectral peaks at the fundamental frequency at all three different spans are lower in the upscaled case (TTM4:3) and higher in the downscaled case (TTM5:3). The differences of peak amplitudes are most pronounced at 90% span, whereas the differences near the rotor hub are reduced.

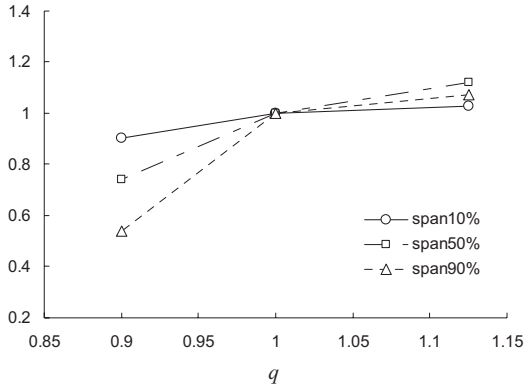

Fig. 9: Peak amplitudes of pressure fluctuations at the fundamental vane frequency at 10% axial chord, normalized by the corresponding values for the TTM3:2.

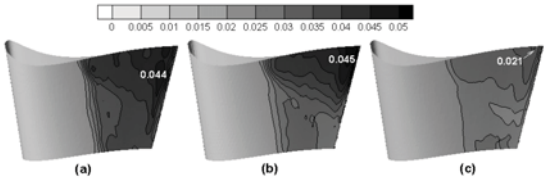

Fig. 10: Iso-contours of the standard deviation of static pressure fluctuations (normalized by the total inlet pressure) on the suction side of the vane: (a) TTM4:3, (b) TTM3:2, (c) TTM5:3.

Figure 10 shows iso-contours of the standard deviation of pressure fluctuations on the suction side of the vane, where pressure fluctuations on the vane surface are strongest. The strongest fluctuations occur near the trailing edge and toward the stator casing. A possible explanation for this observation can be related to the suggestion of Göttlich et al. (2006) that the vane trailing edge shock is reflected on the oncoming blades and moves upstream impinging on the suction side of the vane near the trailing edge. The maximum pressure fluctuations on the vane were significantly weaker than those on the blade. Curiously, the strongest pressure fluctuations on the vane were observed for the unscaled case, whereas the pressure fluctuations for the downscaled case were only slightly lower and for the upscaled case significantly lower.

Figure 11 shows the spectral amplitude of the static pressure fluctuations of the suction side of the stator vane at 90% span and 95% axial chord. Downsizing the blades (TTM5:3) increased the peak frequencies of the pressure fluctuations on the vane, while upsizing the blades (TTM4:3) decreased them.

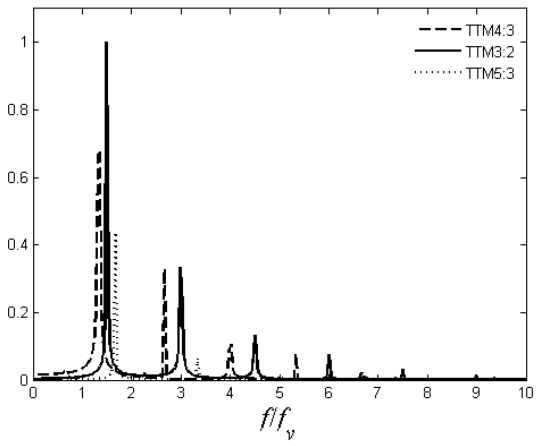

Fig. 11: Spectral amplitude (normalized by its value in the TTM3:2 case at the fundamental stator vane passing frequency) of pressure fluctuations on the suction side of a stator vane at 90% span and 95% axial chord; □ TTM4:3, ○ TTM3:2, Δ TTM5:3.

CONCLUSIONS

Unsteady simulations of flow in a single-stage axial turbine have been conducted with the objective to investigate the effects of rotor blade scaling on the time-averaged turbine performance and on parameters that influence vibratory stresses on the rotor blades. Besides the unscaled case, two scaled rotor blades were considered: blades upscaled by 12.5% and blades downscaled by 10%. Rotor blade scaling was performed by keeping the rotor solidity, the ratio of the tip clearance height and the blade height, and the axial gap size the same for all examined cases.

Comparison of the results for the three cases considered demonstrated that differences in time-averaged turbine performance indicators (i.e., the normalized turbine power, the total-to-total turbine efficiency, the total pressure ratio, and the total temperature drop across the turbine stage) were negligible. However, differences in the time-averaged surface pressure distributions on both the blades and the vanes were noticeable, as time-averaged pressure generally increased with increasing blade count.

It has been noted that the vane trailing edge shocks were largely responsible for the unsteady blade loading of the blade suction side, with the strongest pressure fluctuations occurring near the leading edge and towards the root of the blade. The peak spectral amplitudes of the pressure fluctuations in this region were intensified as the blade count decreased, although the frequencies of these peaks were independent of the blade count.

The pressure fluctuations on the vane were weaker than on the blade, with the strongest fluctuations occurring near the vane trailing edge and toward the stator casing. The strongest fluctuations were observed for the unscaled case, whereas the peak frequencies of the pressure fluctuations on the vane were reduced as the blade count was reduced.

ACKNOWLEDGEMENTS

Financial support for this work was provided by Pratt and Whitney Canada Ltd and the Natural Sciences and Engineering Research Council of Canada. The authors are grateful to Prof. S. Sjolander of Carleton University for his valuable advice on early results of this study.

REFERENCES

Clark, J.P. and Grover, E.A., 2007, "Assessing Convergence in Predictions of Periodic-Unsteady Flowfields", *ASME Journal of Turbomachinery,* Vol. 129, pp. 740-749.

Clark, J.P., Stetson, G.M., Magge, S.S., Ni., R.H., Haldeman, C.W., Jr., and Dunn, M.G., 2000, "The Effect of Airfoil Scaling on the Predicted Unsteady Loading on the Blade of a 1 and ½ Stage Transonic Turbine and a Comparison with Experimental Results", ASME 2000-GT-0446, *Proceedings of the IGTI, ASME TURBO EXPO 2000*, 8-11 May, Munich, Germany.

Göttlich, E., Neumayer, F., Woisetschläger, J., Sanz, W., and Heitmeir, F., 2004, "Investigation of Stator-Rotor Interaction in a Transonic Turbine Stage using Laser-Doppler-Velocimetry and Pneumatic Probes", *ASME Journal of Turbomachinery*, Vol. 126, pp. 297-305.

Göttlich, E., Woisetschläger, J., Pieringer, P., Hampel, B., and Heitmeir, F., 2006, "Investigation of Vortex Shedding and Wake-Wake Interaction in a Transonic Turbine Stage using Laser-Doppler-Velocimetry and Particle-Image-Velocimetry", *ASME Journal of Turbomachinery*, Vol. 128, pp. 178-186.

McBean, I., Hourigan, K., Thompson, M., and Liu, F., 2005, "Prediction of Flutter of Turbine Blades in a Transonic Annular Cascade", *ASME Journal of Fluids Engineering*, Vol. 127, pp. 1053-1058.

Menter, F.R., 1991, "Influence of Freestream Values on k-ω Turbulence Model Predictions", *AIAA Journal*, Vol. 30, pp.1657-1659.

Rai, M.M., 1987, "Navier-Stokes Simulations of Rotor/Stator Interaction using Patched and Overlaid Grids", *ASME Journal of Propulsion and Power,* Vol. 3, pp. 387-396.

Rai, M.M. and Madavan, N.K., 1990, "Multi-Airfoil Navier-Stokes Simulations of Turbine Rotor-Stator Interaction", *ASME Journal of Turbomachinery,* Vol. 112, pp. 377-384.

Yao, J., Davis, R. L., Alonso, J.J. and Jameson, A., 2002, "Massively Parallel Simulation of the Unsteady Flow in an Axial Turbine Stage", *ASME Journal of Propulsion and Power*, Vol. 18. pp. 465-471.